The Electrochemical Society
Advancing solid state & electrochemical science & technology

Comprehensive Electrochemical, Calorimetric Heat Generation and Safety Analysis of $Na_{0.53}MnO_2$ Cathode Material in Coin Cells

Comprehensive Electrochemical, Calorimetric Heat Generation and Safety Analysis of Na$_{0.53}$MnO$_2$ Cathode Material in Coin Cells

Ijaz Ul Mohsin,[z] Carlos Ziebert, Magnus Rohde, and Hans Jürgen Seifert[*]

Institute for Applied Materials—Applied Materials Physics (IAM-AWP), Karlsruhe Institute of Technology, Karlsruhe, Germany

The sodium ion cells were assembled by using Na$_{0.53}$MnO$_2$ as cathode material, pure sodium metal as anode in case of half coin cells and coconut shell-derived hard carbon in case of full coin cells. Cyclic voltammetry, galvanostatic charge-discharge, and self-discharge analysis were conducted. A good rate capability, capacity retention, coulombic efficiency (99.5%), reproducibility and reversible Na-ion intercalation revealed a satisfactory performance of this cathode material. The safety related parameters including the heat generation during charging-discharging and thermal abuse tests have been executed by the means of sophisticated calorimetry instruments. It was observed that during the charging process less heat was generated than during discharging process. The exothermic reactions during thermal runaway were identified by using an accelerating rate calorimeter and pressure measurements during this thermal abuse test were performed as well. The thermal runaway of full coin cells occurred beyond 190 °C with a temperature rate (dT/dt) of 2.5 °C min^{-1}. Such detailed analysis of heat generation and thermal abuse helps finding new and quantitative correlations between different critical thermal and safety related issues in future post Li batteries that are a prerequisite for the design of safer batteries, the safe upscaling and for the adaptation of the thermal management system.

Currently, limited Li metal reserves in the Earth's crust and increasing prices of lithium sources make it imperative to develop alternative rechargeable battery technologies for lithium-ion batteries (LIBs), especially in the field of large-scale electrical energy storage. The abundance of sodium with negative potential of −2.71 vs standard hydrogen electrode (SHE) has similar kinetics mechanism to lithium. Therefore, Na-ion batteries are emerging as an attractive alternative to state-of-the-art LIBs.[1–3] Similar to other energy storage devices, cathodes act as a vital component, which determines the electrochemical characteristics, safety and of course cost of SIBs.[4,5] Considerable attention has been paid to exploring ideal cathode materials with high specific capacity, high-rate capability and long cycle life in the last couple of years.[6–9] Several classes of cathode materials, such as oxides or phosphates (NASICON) have been intensely investigated as suitable cathodes for SIB.[6–9] The cathode materials with layered structure with P2-type and O3-type are regarded as two of the promising classes of cathodes for SIBs because of their high specific capacities, broad range of working voltage and simple synthesis process.[10,11] In comparison to O3-type layered compounds, P2-type cathodes have open prismatic paths within metal oxide slabs and facilitate direct sodium-ion diffusion, indicating better high-rate properties than O3-type.[12] Nevertheless, it usually "suffers" from the P2–O2 phase transformation when Na-ions are extracted. This phenomenon introduces significant changes in the crystal volume and causes a reduction of the reversible capacity.[13]

As negative electrode for SIBs, three classes of materials are mainly investigated. However, phosphorus has also recently received increasing attention.[14] Titanium oxide based materials, such as TiO$_2$ polymorphs and lithium titanate (LTO) reveal a stable long-term cycling behaviour but show comparatively low specific capacities and high operating potentials (0.7 V vs Na/Na+). In addition to that, TiO$_2$ materials show a very high irreversible capacity loss in the first cycle, which aggravates their application in full cells.[15] The second class includes materials that undergo reversible de-alloying/alloying with sodium and deliver much higher specific capacities (e.g. Sn, Sb). Unfortunately, these materials suffer from large volume changes upon cycling and lead to structural degradation and capacity reduction. On top of it, Sn and Sb are toxic,

not abundant and expensive. That is the reason these metals are not suitable for large-scale stationary energy storage.[13] In consequence, the most promising negative electrodes nowadays are probably carbonaceous materials[16,17] and non-graphitizable carbon, so-called hard carbon (HC) is one of the most promising anode materials in case of SIBs. Hard carbon exhibits very good electrochemical performance in combination with many cathode materials in sodium-ion cells.[18,19] The combination of hard carbon with layered oxides is very attractive in terms of delivered energy. Current focuses are on the development of sodium-ion cells with combination of P2 layered oxide cathode Na$_{0.53}$MnO$_2$ and coconut shell-derived commercial hard carbon anode. Special prominence is given in this work to fully describe this system in terms of energy efficiency of both cathode and anode materials. Additionally, total heat generation and cycling procedure were investigated for both half and full cells. Finally, the exothermal reactions were identified by a Heat-Wait-Seek test in accelerating rate calorimeter (Thermal Hazard Technology (THT), UK) for detailed investigation of sodium-ion cells, as thermal reactions identification is important for optimization and design of battery packs. SIBs are interesting alternatives to mature LIBs, as they deliver good electrochemical performance in similar kinetics mechanism. Although, SIBs are still premature and in an early stage of development and further optimization is certainly required. However, for stationary energy storage systems with a long-running operation, the safety is the primary concern.

Experimental

Electrochemical measurements.—The commercial positive electrode 90 wt.% Na$_{0.53}$MnO$_2$ (NEI-Corp. USA) with average particle size (d$_{50}$) = 2 μm was mixed with 5 wt.% Polyvinylidene fluoride (PVDF), 5 wt.% carbon black (Super C65), in N-Methyl-2-pyrrolidon (NMP) solvent in order to have a homogenous slurry. The slurry was coated on Al-current collector foil (19 μm thickness) with the help of a doctor blade. After drying and calendaring, electrode disks of 13 mm diameter were punched. Similarly, the anode slurry was prepared by mixing 90 wt.% of hard carbon, 5 wt.% of conductive carbon black (Super C65), and 5 wt.% PVDF binder (same as for the cathode).
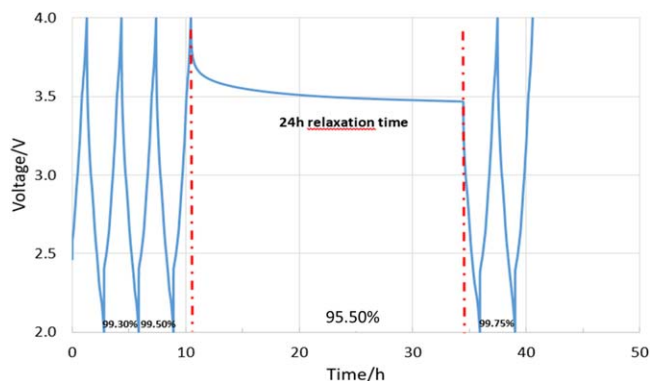
Sodium metal and commercial coconut-shell derived hard carbon (HC) with specific surface area of 4 m^2 g^{-1}, average particle size (d$_{50}$) = 9 μm and interlayer spacing d$_{002}$ > 0.380 nm, as anode

*Electrochemical Society Member.
[z]E-mail: ijaz.mohsin@kit.edu
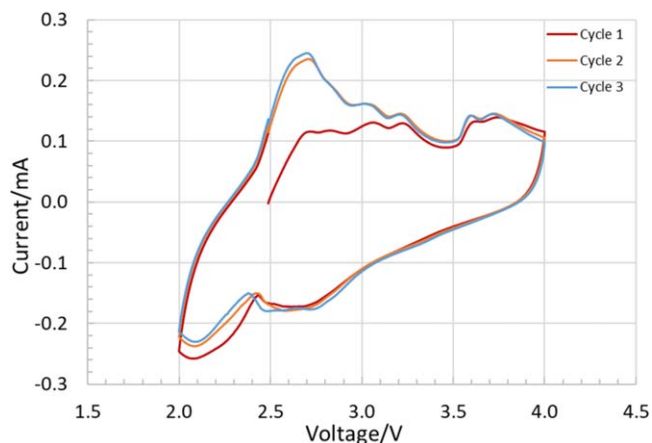
Figure 1. Cyclic voltammetry (CVs) of $Na_{0.53}MnO_2$ with sweep rate of 0.5 mV s^{-1}.

Figure 2. Self discharge phenomenon for $Na_{0.53}MnO_2$ vs Na Coin cell for 24 h.

electrode were implemented in CR2032-type half and full coin cells, respectively. As electrolyte 1 M NaClO$_4$ in EC:DMC: EMC (vol, 1:1:1) plus 2% FEC in volume was used. The electrochemical properties were characterized by using BioLogic instruments at 25 °C for cyclic voltammetry (CV), galvanostatic charge-discharge, rate capability and cycleability for testing.

To develop a sodium-ion cell it is important to study the performance of the two electrode materials separately by profound characterization against sodium metal as anode in half cells. Therefore, the first research step was to investigate the delivered capacity of the two electrode materials and find the suitable mass/ capacity electrode-balancing ratio needed for the development of sodium-ion full cells.

The operating voltage range of the full cell was set to 2.0–4.0 V, because it is known from previous studies,[20] that this results in the most stable long-term cycling behaviour. The electrode balancing was then adjusted to keep the cathode approximately within the 4.0–2.0 V (vs Na/Na$^+$) range and the anode between 0.01 and 2.0 V (vs Na/Na+). The specific practical capacities of the anode and cathode were known from half-cell tests and have been utilized to determine the mass balancing of the cathode and anode. The tests were performed at a C-rate of 0.1C with respect to the cathode/anode weight. The capacity balancing and the activation procedure were adjusted with respect to the selected electrode materials, especially considering their first cycle irreversible capacity. An excess cathode material (sodium source) was applied to account for sodium consumption during formation of the solid electrolyte interface (SEI) at the anode side.

Heat generation analysis.—To investigate the total heat genera-tion, fresh half-coin cells ($Na_{0.53}MnO_2$ vs Na) with 2.8 mAh capacity and full-coin cells with 1.15 mAh capacity ($Na_{0.53}MnO_2$ vs hard carbon) were assembled. The operation voltage range was set between 2.0 V and 4.0 V. The total heat generation was investigated by an MS80 3D Tian-Calvet calorimeter (Setaram Instrumentation, France) under isothermal conditions at 25 °C. The cycling data were recorded via a PicoLog instrument. The constant current, constant voltage (CCCV) with current (I) < C/20 or time > 60 min test profile were employed both in charging (4.0 V) and discharging (2.0 V) with a rate of 0.2C. The 10 h relaxation period was introduced in between each charge and each discharge cycle to reach thermal equilibrium.

Thermal abuse test.—Accelerating rate calorimetry is widely adopted as a thermal characterization method for hazardous thermal runaway reaction studies of batteries.[21,22] On full-coin cells ($Na_{0.53}MnO_2$ vs HC) safety tests were performed using an es-ARC (Thermal Hazard Technology, UK). A stack of 2 coin cells were placed in the calorimeter chamber to get sufficient thermal signal. The chamber has heaters and thermocouples located in lid, bottom and sidewalls, that adjust the required ambient conditions that are characterized by the related thermocouples. The control or so-called bomb thermocouple was sandwiched between two coin cells, which were wrapped with glass cloth tape. The measurement profile for the Heat-Wait-Seek (HWS) test was set in the range of 30 °C−550 °C with a sensitivity threshold detection limit of 0.02 °C min^{-1}. The coin cells were heated up stepwise by 5 °C steps and after each "*Heat*" step the system maintained the temperature for 15 min, which is called "*Wait*"-mode to stabilize the temperature in the calorimeter. At the end of the "*Wait*"-mode, the temperature change rate (dT/dt) was detected and was compared with the set sensitivity threshold of 0.02 °C min^{-1} ("*Seek*"-mode). If the temperature rate dT/dt is lower than 0.02 °C min^{-1}, the "*Heat*" mode will be continued. As soon as self-heating of the cell is detected to exceed the sensitivity limit, the heaters in the calorimeter chamber im-mediately follow any change of the cell temperature preventing the heat transfer to the chamber. In this so-called "*Exotherm*" mode, the cell is heating up more and more until a thermal runaway occurs or the chemicals for this exothermal reaction are completely consumed. Before the measurements, the coin cells were charged to a state of charge (SOC) 100% with constant current, constant voltage (CCCV) method with a rate of 1/40C.

In addition pressure measurements were performed on single fully charged (SOC 100%) sodium full-coin cells ($Na_{0.53}MnO_2$ vs HC). For that purpose, the coin cell was placed in a small canister designed for CR2032 coin cell pressure measurement. A thin ceramic disc was placed on one side of the coin cell before sealing to avoid a short circuit. The canister was coupled to a capillary tube leading to a pressure transducer. The canister containing the coin cell was placed in the es-ARC and was heated up with a constant heating rate of 5 °C min^{-1} to 550 °C temperature. During the test, the pressure generation after the opening of the coin cell was recorded.

Result and Discussion

Full cell development.—The cathode material performance was studied by assembling half-cells. The cyclic voltammetry with sweep rate of 0.5 mV s^{-1} was executed and different redox peaks were identified as shown in Fig. 1. The redox peaks were reproducible and also showed good repeatability.

The cathodic and anodic peaks indicated the complicated process of Na insertion/extraction.

The lower potential range (2.5–2.9 V) represented Mn^{+3}/Mn^{+4} redox reaction resulting from extraction/insertion of Na as also reported in literature.[23,24] At higher potential range (3.5–4.0 V); structural phase oxidation was associated with the formation of the O2 phase at low Na content as Hasa et al. also mentioned in their investigation of P-type layered sodium transition metal-based oxides
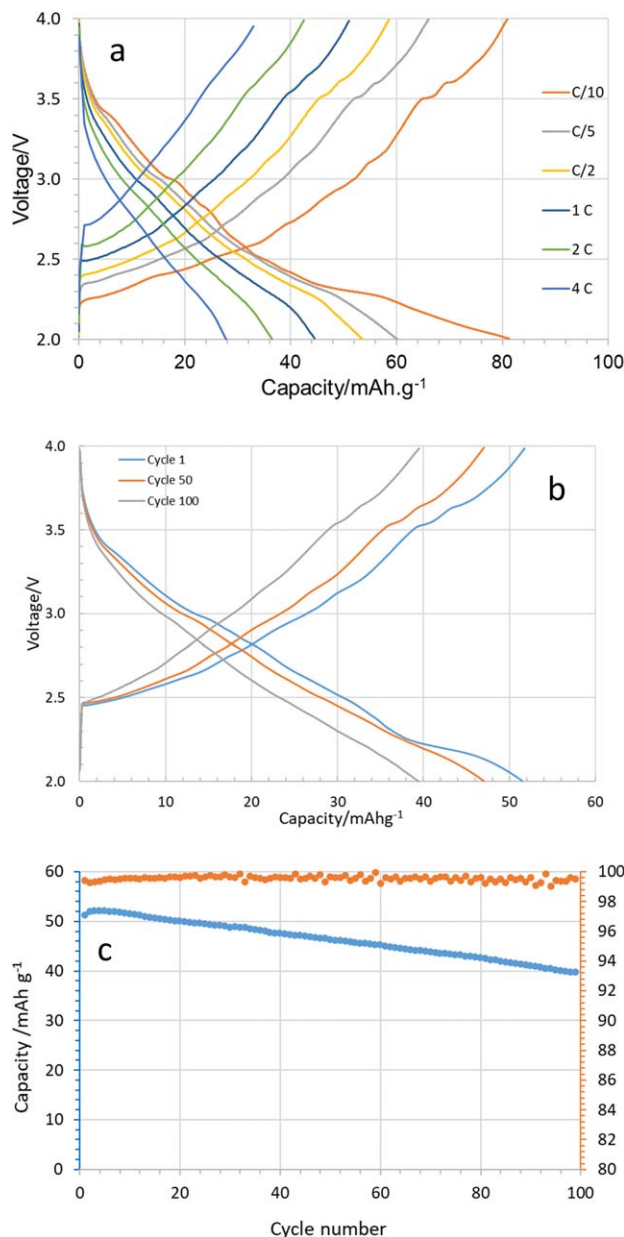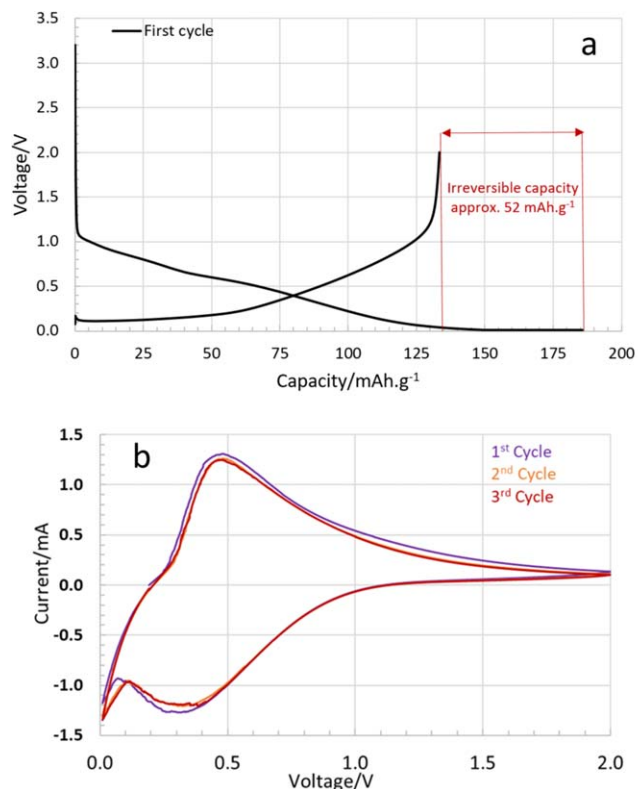
Figure 3. Test result for $Na_{0.53}MnO_2$ in half cell; (a) rate capability test of $Na_{0.53}MnO_2$ cathode (positive electrode) vs Na in half cell, (b) Cycleability test of $Na_{0.53}MnO_2$ cathode vs Na in half-cell (100 Cycles at 0.5C rate), (c) capacity depletion and coulombic efficiency of $Na_{0.53}MnO_2$ cathode vs Na in half-cell (100 Cycles at 0.5C rate).

Figure 4. Test results for hard carbon in half-cell; (a) capacity loss (irreversible capacity) in first cycle (0.1C rate) of hard carbon vs Na in half-cell, (b) cyclic voltammetry (sweep rate 0.5 mV s^{-1}) of hard carbon vs Na in half-cell.

Na_xMO_2 (M = Ni, Fe, Mn) as a cathode material.[25] Small cathodic and anodic peaks correspond to the rearrangement and migration of Na ion vacancies and this was found satisfactory to the sodium layered oxide material $Na_{0.67}Mn_{1-x}Mgx_O_2$ ($0 \leqslant x \leqslant 0.2$) investigation reported previously.[26,27]

As next step the self-discharge phenomenon of the battery was studied to observe the stability of the battery and capacity retention (SOC 100%) in case of a heat generation test where a relaxation period (10 h) was introduced between charging and discharging periods.

The self-discharge procedure is mostly applied to evaluate the side reactions of the electrodes as well.[28] The self-discharge measurement was performed on half-cells as follows: the half coin cell was cycled for three times at 0.5C rate firstly, and then charged to 4.0 V (constant current) with 0.5C rate, standing for 24 h at 25 °C temperature (Fig. 2). Finally, it was discharged to 2.0 V (constant

current) with 0.5C rate followed by a complete cycle. As shown in Fig. 2, after relaxation of 24 h, the coulombic efficiency increased slightly to 99.75%, although the potential decreased to 3.5 V indicating the smaller self-discharge behaviour approximately of 4% (i.e. efficiency decreases to 95.50% after relaxation).

To see the charge-feasibility of sodium based cathode battery, rate capability test was performed with various C-rates as shown in Fig. 3a. When the C-rate is increased a decrease in the capacity performance is the usual observed phenomenon. Although, the cathode material has a low capacity (~65% achievable capacity from theoretical capacity ~136 mAh.g^{-1}), still it showed a very good rate capability. The half-coin cell was cycled 100 times with a 0.5C rate. The result is presented in Fig. 3b. The fading in capacity after 100 cycles is due to the structure change in the material and the battery retained a state of health (SOH) 80% with almost more than 99.50% coulombic efficiency (Fig. 3c).

The cathode material showed good electrochemical performance in half-cell investigations.

An anode material not only needs to have a high specific capacity, but also a relatively low voltage potential to enable a high energy density in full cells. Therefore, the commercial coconut shell-derived hard carbon was utilized to develop a full cell. Before development, electrochemical characterization was examined in half-cells against Na metal in the range of 0.01–2.0 V with 0.1C rate. The typical discharge curve of HC against sodium metal is composed of a slope region (intercalation–pore filling mechanism) and a plateau region (adsorption–intercalation–pore filling mechanism).[29]

The first cycle (0.1C rate) irreversible capacity loss of hard carbon, due to SEI formation, was about 52 mAhg^{-1} for the hard carbon (Fig. 4a) with first cycle coulombic efficiency of around 71% (0.01–2.0 V vs Na/Na$^+$). In cyclic voltammetry (Fig. 4b), it was observed that most of the capacity was achieved below 1.0 V and sharp peaks were found at 0.01–0.2 V, which correspond to the
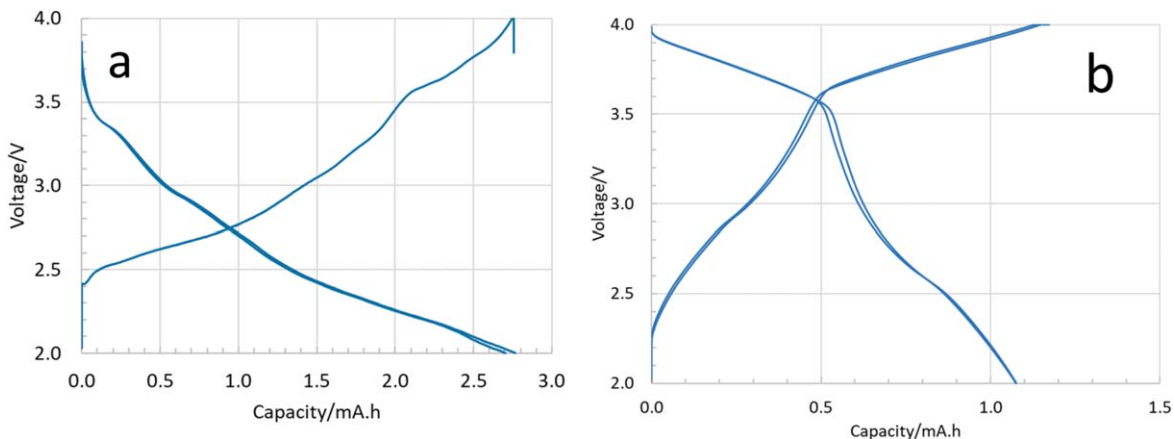
**Figure 5.** High powder loading half (a)-and full (b) coin cells with respective capacities at C/40 rate.

insertion and extraction of the sodium ions between disordered carbon layers and are related to adsorption intercalation mechanisms in that plateau. The replication of the voltammetry curves shows good consistency of the charge-discharge loops.

In the voltage range of 4.0 to 2.0 V, the cathode material $Na_{0.53}MnO_2$ delivered a discharge capacity of $\sim$84 mAh.g^{-1} at 0.1C rate (Fig. 3a) and the anode material hard carbon (HC) $\sim$185 mAh.g^{-1} at 0.1C rate (first cycle, Fig. 4a), which are the measured capacities in the sodium-metal half-cells. Balancing of the capacities of the electrodes was made by considering the first cycle irreversible capacity loss of the anode at 0.1C rate, which yielded a cathode/anode capacity ratio of approximately 2.2: 1. Based on this capacity ratio, respective electrode sheets were coated on aluminium foil by adjusting the layer thickness accordingly followed by full-coin cells development for further safety analysis.

Heat generation.—For heat generation test, high powder cathode material loading of 28 g cm^{-2} half cells (Fig. 5 left) and full coin cells with anode material loading of 13 g cm^{-2} (Fig. 5 right) were assembled to get sufficient heat flow signal with certain slow charging/discharging rates i.e. 0.2C in MS80 calorimeter. The coin cells were formatted with C/40 rate in order to get maximum capacities i.e. 2.8 mA.h in case of half-cell (a) and 1.15 mA.h in full-cell (b) as depicted in Fig. 5. For the high powder loading cells, slow charging rates are beneficiary in achieving maximum capacities.

Figure 6a provides an insight into the in-operando heat flow measurement during cycling of the half coin cell with 0.2C rate at 25 °C. The experimental data of each cycle are reproducible under the same operating conditions. As a result, one of the 3 cycles was extracted for further detailed analysis. During the charging process, voltage and charge capacity of the battery gradually increase, mainly due to the migration/shuttling of sodium ions from positive electrode to negative electrode. When the voltage reaches the upper and lower boundary at 4.0 V and 2.0 V (charge/discharge cut off), no current is flowing into the system. At these stages, Joule heat and reversible heat of the cells are zero.[30] However, due to the internal temperature gradient generated by relative high C rate cycling (higher material loading than usual), the heat produced within the cell is still slowly released to the outside, which is known as residual heat.[31] It is a general statement that the total heat generation in charging and discharging increases with rising current rate and thickness.[32] The electrode thickness is more dominant for internal heat generation than the current rate because of lengthening insertion and extraction path of sodium ions, which produce a larger concentration gradient of sodium ions in the direction perpendicular to the surface and significantly increase the polarization heat. Secondly, the cell has a higher capacity because of thicker electrode sheet.

Besides in full-cell, when SOC is close to 100% (fully charge) or 0% (fully discharge), the heat release rate of the cell becomes larger.
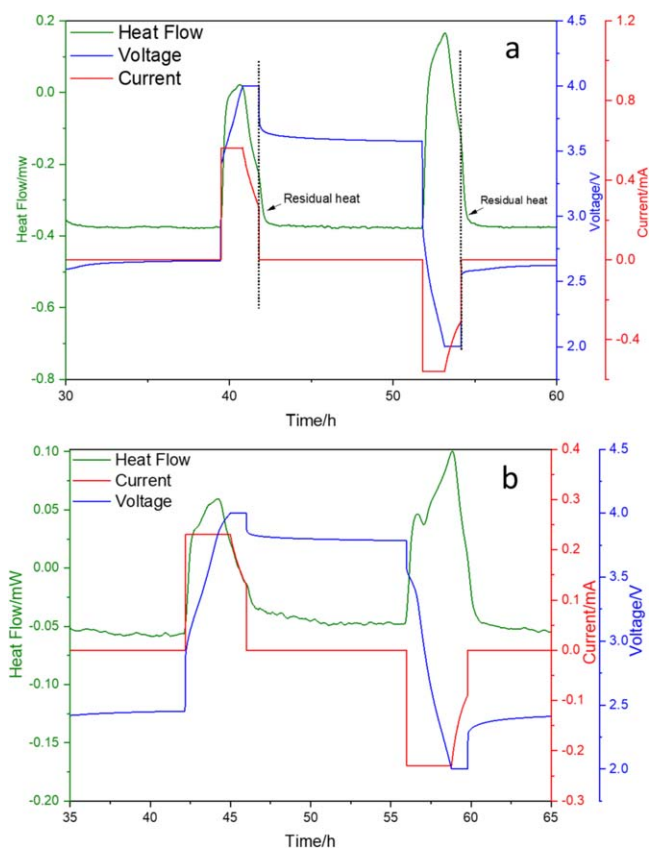

Figure 6. In-operando heat generation results; (a) total heat generation in $Na_{0.53}MnO_2$/Na half-cell during charging & discharging at 0.2C rate, (b) total heat generation in $Na_{0.53}MnO_2$/HC full cell during charging & discharging at 0.2C rate.

Nevertheless, a significant decrease in the heat generation can be observed in the middle of the discharge process in the full-coin cell (Fig. 6b), which is mainly due to the tendency of concentration polarization resistance. While in the discharge phase, the voltage decrease with the discharging time and heat release rate shows a tendency of increasing smoothly followed by a rapid increase that was not observed in the half-cell probably due to Na metal as anode material i.e. sufficient Na source availability. Near the end of the discharging process in a full-cell, a sharp peak of heat flow appears which corresponds to a higher internal resistance of the cell. When the SOC becomes lower, the polarization within the battery get

severe and the internal resistance increase significantly resulting in an elevation of the irreversible heat inside the battery.

The heat generation data measured in half-and full-coin cells are listed in Table I. It was found that in the discharging phase, more heat was generated as in the charging phase due to irreversible heat generated by the internal resistance of the system.

Thermal abuse test.—The test data obtained from the ARC heat-wait-seek test are presented in Fig. 7a and the corresponding self-heating rate (°C min^{-1}) and pressure (bar) are plotted against the temperature (°C) in Fig. 7b. Figure 7a demonstrates the results of thermal runaway measurements of stacks of two fully charged full-coin cells. The tested cells reach a maximum temperature of 550 °C of the calorimeter (ARC). We can see clearly that three exothermic reactions take place at 162 °C (stage 1), 185 °C (stage 2) and 190 °C (stage 3) respectively, where the system switched to the *"Exotherm"* mode and the temperature rate exceeded the defined threshold sensitivity limit of 0.02 °C min^{-1}. However, the detected temperature rates in the cells below the onset temperature revealed the small exothermic reactions during heating. Stage 1 at 160 °C–162 °C could be the decomposition of the solid electrolyte interface (SEI) layer, because Xia et al.[33] also measured the thermal stability of an O3-type layered structure cathode material $NaNi_{0.33}Fe_{0.33}Mn_{0.33}O_2$ with accelerating rate calorimetry and found that the onset temperature of exothermic reaction induced by the thermal decomposition of the SEI is about 166 °C. However, they used 1.0 M $NaPF_6$ (PC: EMC, 1:1 v/v + 2 wt.% FEC) as electrolyte and the SEI stability could slightly differ from our study. That could be a reason why Xie et al.[34] observed a rapid exothermal acceleration reaction at a peak temperature of 312 °C and SEI thermal decomposition at 166 °C. To see the reaction mechanism between HC (as anode material) and electrolyte, the sodiated HC and fresh HC with electrolyte were assembled in coin cells without positive material and stack of 2 coin cells of each were tested in similar manner in accelerating rate calorimeter and results were depicted in Fig. 7C. It was observed that the sodiated HC showed early exothermic reaction at 190 °C than fresh HC at 230 °C, which was due to sodium laying in HC leading to increase the reactivity to electrolyte which was seen clearly in full cells at second stage (185 °C) of exothermic reaction (electrode/electrolyte reaction). The relative slightly aggressive self-heating rates were found in sodiated HC than the fresh HC but noticeable trend of self-heating rates were similarly. Wang et al.[35] reported on Lithium-based battery that the solid electrolyte interphase (SEI) layer on the anode side begins to decompose at 90 °C resulting in self-heating initiation. Perea et al.[36] perceived as well that at 137 °C the exothermic reactions occurred between electrolyte and electrodes in case of lithium batteries. These studies support the occurrence of exothermal reaction trigger later than Lithium-based batteries. The SEI film could be composed of stable and metastable components such as Na_2CO_3 and (CH_2OCO_2Na), depending on the composition of the carbonate-based electrolyte as reported in the literature for Lithium-based batteries[37,38] and these compounds could thermally decompose further. It was suggested in another study[39] that the thermal runaway in Na-ion batteries (SIBs) occurs via a similar mechanism to that reported for Li-ion cells and thermal runaway event initiates at a higher temperature in Na-ion cells compared to LIBs. Xia et al.[33] evaluated another layered structure $NaCrO_2$ via ARC and they found that $Na_{0.5}CrO_2$ (SOC 100%) has no obvious reactivity until 350 °C. However, in the lithium case, $Li_{0.5}CoO_2$ showed an exothermic behaviour below 300 °C.
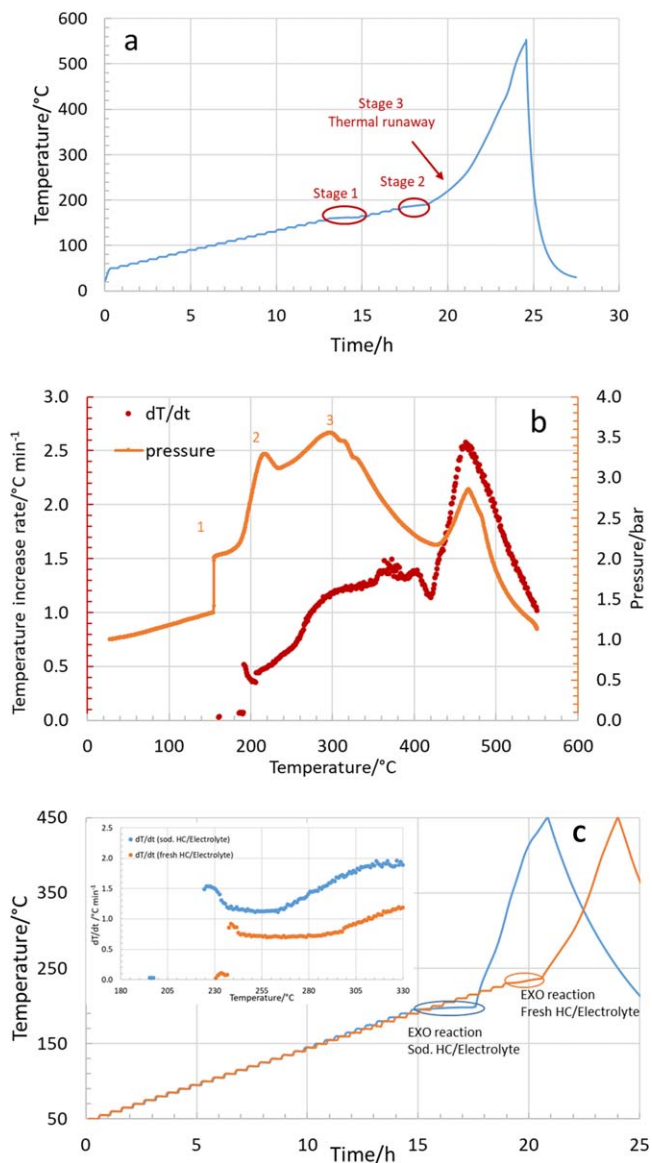
Figure 7. Thermal abuse test results: (a) temperature vs time curve during a Heat-Wait-Seek test on a stack of two full coin cells of $Na_{0.53}MnO_2$/HC at SOC 100%, (b) temperature increase rate and pressure vs temperature curve on a stack of two full coin cells of $Na_{0.53}MnO_2$/HC at SOC 100%, (c) Heat-Wait-Seek test on a stack of two sodiated HC and two fresh HC with electrolyte and self-heating rate.

According to his study, SIBs thermal runaway events trigger later than LIBs.

After SEI degradation, the electrodes are no longer protected from contact with the electrolyte, thus, the exothermic reaction continues due to the direct reaction of the electrode material with the electrolyte components. This can be seen in the temperature range of 180 °C–185 °C, where an exothermic reaction was detected. Beyond 190 °C, self-heating rate continued to increase and the behaviour was dominated by the combustion reaction of the

Table I. Heat generation data during charging/discharging of half- and full cell with 0.2C rate.

Coin cell	Current flow	Capacity mA.h	Heat generation charge (J)	Heat generation discharge (J)
Full-cell (1.15 mAh)	0.2C	0.82 ± 0.04	1.31 ± 0.03	1.49 ± 0.01
Half-cell (2.8 mAh)	0.2C	1.16 ± 0.01	2.65 ± 0.03	3.70 ± 0.03

organic based electrolyte. That was observed clearly in the internal pressure build-up and the opening of the coin cell casing. The pressure development in battery appears before the occurrence of reactions that can lead to thermal runaway prior to triggering a dangerous stage.[40] Although, the cell opens at 155 °C and a sharp pressure increase was measured (stage 1). As the internal pressure of the coin cell could not be measured directly with the existing setup that is why after bursting of the coin cell, the pressure was recorded with a ramp-up temperature profile instead of HWS profile i.e. the onset point could differ. The pressure increase pattern was similar to that of the temperature increase rate until stage 2 and then both slightly decrease. Above 320 °C in Fig. 7b, the temperature increase rate promptly increased due the start of the thermal decomposition of the electrolyte followed by oxygen release from cathode material[41] resulting in a pressure rise up to stage 3. Beyond 400 °C, decrease in dT/dt is the due to the melting of sealing ring of coin cells and shows some cooling effect as an endothermic phase. Beyond 420 °C, the sealing ring of coin cells start to decompose resulting in raising pressure sharply that was also noticed in thermal runaway test i.e. sharp increase in temperature rate. The thermal runaway events of fully charged coin cells reached 550 °C with a maximum temperature rate of 2.5 °C min^{-1}. Golubkov et al.[42] and Abraham et al.[43] conducted a thermal runaway study on commercial lithium cells (18650) with active cathode materials of $LiFePO_4$, $Li(Ni_{0.45}Mn_{0.45}Co_{0.10})O_2$, a blend of $LiCoO_2$ + $Li(Ni_{0.50}Mn_{0.25}Co_{0.25})O_2$ and $LiNi_{0.8}Co_{0.15}Al_{0.05}O_2$. Each commercial cell was showing various onset temperatures of 150 °C, 170 °C, 195 °C, and 84 °C respectively. Hence, thermal runaway strongly depends on the electrode materials intrinsic stability as well. That could be a possible explanation, why we observed different onset temperatures of thermal runaway events in our study.

The abuse test was not executed on half-cells ($Na_{0.53}MnO_2$/Na) because of the low melting point (97 °C) of sodium metal.

Conclusions and Outlook

The sodium based cathode material half-and full coin cells electrochemical performances have been profoundly investigated and the half-cell exhibited a discharge capacity of 84 mAh g^{-1} at a discharge rate of 0.1C in case of cathode material. The cathode material delivered a good rate capability and good capacity retention (approx. > 80% after 100 cycle at 0.5C). The coulombic efficiency (99.5%), reproducibility and reversible Na-ion intercalation revealed a satisfactory performance of the cathode material. The full-coin cell was developed against a promising anode material (HC) by balancing the cathode/anode capacity ratio. In half-and full cells heat generation was measured and it was observed that during the charging process less heat was generated than during the discharging process. Of course, the irreversible heat generation is higher in case of discharge, which corresponds to a higher internal resistance of the cells. Different exothermal reactions were identified in a full cell by the Heat-Wait-Seek method. The thermal runaway of full coin cells occurred beyond 190 °C and reached up to 550 °C with a temperature rate (dT/dt) of 2.5 °C min^{-1}. The measured pressure curve after bursting of the coin cell has supported the reaction mechanism that occurs during thermal runaway event beyond 190 °C i.e. thermal decomposition of electrolyte, reaction between electrolyte and electrode materials and thermal degradation of cathode material. The safety preliminary studies of SIBs could be useful for the future research in sodium battery technology. The pressure development in battery predicts the occurrence of thermal runaway prior to trigger a dangerous stage, therefore internal pressure measurement will be taken into account as well as exhaust gas analysis for further upscaling research in case of pouch cells. The exothermal reactions in pouch cells shall be compared to the coin cells in the same manner as well. As in pouch cells thermal abuse analysis (temperature increase rate (dT/dt)) are more profound than that of coin cells due to of high material loading yielding a higher capacity.

ORCID

Ijaz Ul Mohsin https://orcid.org/0000-0001-6252-3358

References

1. J.-Y. Hwang, S.-T. Myung, and Y.-K. Sun, *Chem. Soc. Rev.*, **46**, 3529 (2017).
2. K. Z. Jiang, S. Xu, S. H. Guo, X. Y. Zhang, X. P. Zhang, Y. Qiao, T. C. Fang, P. Wang, P. He, and H. S. Zhou, *Nano Energy*, **52**, 88 (2018).
3. P. Mei, Y. V. Kaneti, M. Pramanik, T. Takei, O. Dagc, Y. Sugahara, and Y. Yamauchi, *Nano Energy*, **52**, 336 (2018).
4. R. R. Salunkhe, Y. V. Kaneti, and Y. Yamauchi, *ACS Nano*, **11**, 5293 (2017).
5. R. R. Salunkhe, C. Young, J. Tang, T. Takei, Y. Ide, N. Kobayashi, and Y. Yamauchi, *Chem. Commun.*, **52**, 4764 (2016).
6. Y. Huang, X. Li, J. Wang, L. Miao, C. Li, J. Han, and Y. Huang, *Energy Storage Mater.*, **15**, 108 (2018).
7. Y. You, X. L. Wu, Y. X. Yin, and Y. G. Guo, *Energy Environ. Sci.*, **7**, 1643 (2014).
8. Q. Huang, J. T. Liu, L. Zhang, S. Xu, L. B. Chen, P. Wang, D. G. Ivey, and W. F. Wie, *Nano Energy*, **44**, 336 (2018).
9. X. Zheng, P. Li, H. Zhu, K. Rui, G. Zhao, J. Shu, X. Xu, W. Sun, and S. X. Dou, *Energy Storage Mater.*, **15**, 257 (2018).
10. J. Y. Hwang, T. Y. Yu, and Y.-K. Sun, *J. Mater. Chem. A*, **6**, 16854 (2018).
11. Z. Y. Li, R. Gao, J. Zhang, X. Zhang, Z. Hu, and X. Liu, *J. Mater. Chem. A*, **4**, 3453 (2016).
12. J. Sun, H.-W. Lee, M. Pasta, H. Yuan, G. Zheng, Y. Sun, Y. Li, and Y. Cui, *Nat. Nanotechnol.*, **10**, 980 (2015).
13. D. Kundu, E. Talaie, V. Duffort, and L. F. Nazar, *Angew. Chem.*, **127**, 3495 (2015).
14. T. Chen, L. Pan, T. Lu, C. Fu, D. H. C. Chuab, and Z. Suna, *J. Mater. Chem. A*, **2**, 1263 (2014).
15. E. Irisarri, A. Ponrouch, and M. R. Palacin, *J. Electrochem. Soc.*, **162**, A2476 (2015).
16. S. Wenzel, T. Hara, J. Janek, and P. Adelhelm, *Energy Environ. Sci.*, **4**, 3342 (2011).
17. F. Li and Z. Zhou, *Small*, **14**, 1702961 (2018).
18. Y. Sun, S. Guo, and H. Zhou, *Energy Environ. Sci.*, **12**, 825 (2019).
19. Z. Yuan, L. Si, and X. Zhu, *J. Mater. Chem. A*, **3**, 23403 (2015).
20. J.-K. Kim, Y. J. Lim, H. Kim, G.-B. Chob, and Y. Kim, *Energy Environ. Sci.*, **8**, 3589 (2015).
21. Y.-W. Wang and C.-M. Shu, *Rechargeable Batteries* (Springer, Cham) 419 (2015).
22. B. Lei, W. Zhao, C. Ziebert, A. Melcher, M. Rohde, and H. J. Seifert, *Batteries*, **3**, 14 (2017).
23. J. Xu, D. H. Lee, R. J. Clément, X. Yu, M. Leskes, A. J. Pell, G. Pintacuda, X.-Q. Yang, C. P. Grey, and Y. S. Meng, *Chem. Mater.*, **26**, 1260 (2014).
24. Z.-Y. Li, R. Gao, J. Zhang, X. Zhang, Z. Hu, and X. Liu, *J. Mater. Chem. A*, **4**, 3453 (2016).
25. I. Hasa, D. Buchholz, S. Passerini, and J. Hassoun, *ACS Appl. Mater. Interfaces*, **7**, 5206 (2015).
26. Z.-G. Wu et al., *ACS Appl. Mater. Interfaces*, **9**, 21267 (2017).
27. J. Billaud, G. Singh, A. R. Armstrong, E. Gonzalo, V. Roddatis, M. Armand, T. Rojo, and P. G. Bruce, *Energy Environ. Sci.*, **7**, 1387 (2014).
28. X. Wu, Y. Li, Y. Xiang, Z. Liu, Z. He, X. Wu, Y. Li, L. Xiong, C. Li, and J. Chen, *J. of Power Sources.*, **336**, 35 (2016).
29. D. Saurel, B. Orayech, B. Xiao, D. Carriazo, X. Li, and T. Rojo, *Adv. Energy Mater.*, **8**, 1703268 (2018).
30. D. Bernardi, E. Pawlikowski, and J. Newman, *J. Electrochem. Soc.*, **132**, 5 (1985).
31. T. Wu, H. Chen, Q. Wang, and J. Sun, *J. Hazard. Mater.*, **344**, 733 (2018).
32. C. Liang, L. Jiang, Q. Wang, and J. Sun, *Fire Technol.*, **56**, 2387 (2020).
33. X. Xia and J. R. Dahn, *Electrochem. Solid-State Lett.*, **15**, A1 (2011).
34. Y. Xie et al., *Chem. Mater.*, **30**, 4909 (2018).
35. Q. Wang, J. Sun, X. Yao, and C. Chen, *J. Electrochem. Soc.*, **153**, A329 (2006).
36. A. Perea, A. Paolella, J. Dubé, D. Champagne, A. Mauger, and K. Zaghib, *J. Power Sources*, **399**, 392 (2018).
37. K. Zaghib, M. Dontigny, P. Perret, A. Guerfi, M. Ramanathan, J. Prakash, A. Mauger, and C. M. Julien, *J. Power Sources*, **248**, 1050 (2014).
38. T. Yoon, M. S. Milien, B. S. Parimalam, and B. L. Lucht, *Chem. Mater.*, **29**, 3237 (2017).
39. J. B. Robinson, D. P. Finegan, T. M. M. Heenan, K. Smith, E. Kendrick, D. J. L. Brett, and P. R. Shearing, *J. Electrochem. En. Conv. Stor.*, **15**, 011010 (2018).
40. A. Hofmann, N. Uhlmann, C. Ziebert, O. Wiegand, A. Schmidt, and T. Hanemann, *Appl. Thermal Eng.*, **124**, 539 (2017).
41. I. U. Mohsin, C. Ziebert, M. Rohde, and H. J. Seifert, *Batteries*, **7**, 16 (2021).
42. A. W. Golubkov, D. Fuchs, J. Wagner, H. Wiltsche, C. Stangl, G. Fauler, G. Voitic, A. Thalera, and V. Hacker, *RSC Adv.*, **4**, 3633 (2014).
43. D. P. Abraham, E. P. Roth, R. Kostecki, K. McCarthy, S. MacLaren, and D. H. Doughty, *J. Power Sources*, **161**, 648 (2006).